1   **Reconstructing Antarctic winter sea-ice extent during Marine Isotope**

2   **Stage 5e**

3   Matthew Chadwick[1,2*]; Claire S. Allen[1]; Louise C. Sime[1]; Xavier Crosta[3] & Claus-Dieter

4   Hillenbrand[1]

5   [1.] *British Antarctic Survey, High Cross, Madingley Road, Cambridge, CB3 0ET, UK*

6   [2.] *Ocean and Earth Science, National Oceanography Centre, University of Southampton Waterfront*
7   *Campus, European Way, Southampton, SO14 3ZH, UK*

8   [3.] *Université de Bordeaux, CNRS, EPHE, UMR 5805 EPOC, Pessac, France*

9   *Corresponding author:* machad27@bas.ac.uk, British Antarctic Survey, High Cross, Madingley Road,
10 Cambridge, UK

11 **Abstract**

12 Environmental conditions during Marine Isotope Stage (MIS) 5e (130-116 ka) represent an important

13 'process analogue' for understanding the climatic responses to present and future anthropogenic

14 warming. The response of Antarctic sea ice to global warming is particularly uncertain due to the short

15 length of the observational record. Reconstructing Antarctic winter sea-ice extent during MIS 5e

16 therefore provides insights into the temporal and spatial patterns of sea-ice change under warmer

17 than present climate. This study presents new MIS 5e records from nine marine sediment cores

18 located south of the Antarctic Polar Front, between 55 and 70 °S. We investigate changes in winter

19 sea-ice extent and sea-surface temperatures between the three Southern Ocean sectors. The Atlantic

20 and Indian sector records have much more variable MIS 5e winter sea-ice extent and sea-surface

21 temperatures than the Pacific sector records. High variability in the Atlantic sector winter sea-ice

22 extent is attributed to high glacial meltwater flux in the Weddell Sea while high variability in the Indian

23 sector winter sea-ice extent results from large latitudinal migrations of the flow bands of the Antarctic

24 Circumpolar Current. Overall, these findings suggest that Pacific sector winter sea ice displays a low

25 sensitivity to warmer climates. The different variability and sensitivity of Antarctic winter sea-ice

26 extent in the three Southern Ocean sectors during MIS 5e may have significant implications for the

27 Southern Hemisphere climatic system under future warming.

28   **1. Introduction**

29 Antarctic sea ice is a critical part of the Southern Ocean (SO) and global climate system (Maksym,

30 2019). The vast extent of Antarctic sea ice and its huge seasonal variability (~4-18 x 10^6 km^2 in the

31 present day) have a strong albedo-radiation feedback (Hall, 2004). Brine rejection during sea-ice

32 formation contributes to the production of dense shelf and bottom water masses, which, in turn,

33   influence the strength of global overturning ocean circulation (Abernathey et al., 2016; Rintoul, 2018).

34   Sea-ice cover also regulates heat and gas exchange between the SO and the atmosphere as well as

35   phytoplankton productivity by causing stratification of the upper part of the water column (Goosse

36   and Zunz, 2014) and acting as a physical barrier (Rysgaard et al., 2011) and barrier to sunlight.

37   Modern Antarctic sea-ice extent has shown a rapid decline since 2014 after four decades of gradual

38   expansion (Parkinson, 2019). Within this overall trend there is substantial spatial heterogeneity in

39   regional sea-ice trends, with decreases in the Bellingshausen and Amundsen seas concurrent with

40   increases in the Weddell Sea and Ross Sea sectors (Hobbs et al., 2016; King, 2014; Parkinson, 2019).

41   Alongside the interannual Antarctic sea-ice trends (Parkinson, 2019), there are also trends in seasonal

42   variability, with the Amundsen Sea showing a substantial decrease in summer and autumn sea-ice

43   concentrations but a slight increase in winter and spring sea-ice concentrations (Hobbs et al., 2016).

44   Model simulations are unable to replicate the modern sea-ice changes without reduced regional

45   warming trends (Rosenblum and Eisenman, 2017). Difficulties in reproducing modern sea-ice trends

46   indicate the complexities of the climate dynamics that influence sea-ice extent in the SO today at

47   different timescales (Ferreira et al., 2015; Hobbs et al., 2016; King, 2014; Purich et al., 2016;

48   Stammerjohn et al., 2008).

49   Rising greenhouse gas concentrations are driving current global warming, with polar regions warming

50   twice as fast (0.5 $^{\circ}$C per decade) as the global average (IPCC, 2019) and Antarctic winter sea-ice extent

51   (WSIE) predicted to shrink by 24-34 % by C.E. 2100 (Meredith et al., 2019). However, the very short

52   length of observational records in high latitudes and together with the complexity of the climate

53   system, as mentioned above, limit our understanding of the underlying processes and ability to

54   accurately predict future changes. Past warm periods can help document the amplitude of sea-ice

55   extent reduction and, therefore, help guide our understanding of the impacts of future climate change

56   in polar regions.

57   Interglacial Marine Isotope Stage (MIS) 5e (130-116 ka) is the latest period when global mean annual

58   atmospheric temperatures were warmer than present (~1 $^{\circ}$C; Fischer et al. (2018)) and global sea

59   levels were higher than present (~6-9 m; Kopp et al. (2009)). Summer sea-surface temperatures

60   (SSSTs) in the SO peaked at an average of 1.6 ± 1.4 $^{\circ}$C warmer than present at and north of the modern

61   Antarctic Polar Front during this period (Capron et al., 2014; Shukla et al., 2021). MIS 5e warming is

62   primarily orbitally forced, unlike current and future anthropogenic warming which is driven by rising

63   greenhouse gas concentrations. Whilst MIS 5e cannot be considered a direct analogue for greenhouse

64   gas induced global warming it still represents an important 'process analogue' for understanding

65   climate mechanisms and responses that are active under warmer-than-present climate conditions

66   (Stone et al., 2016).
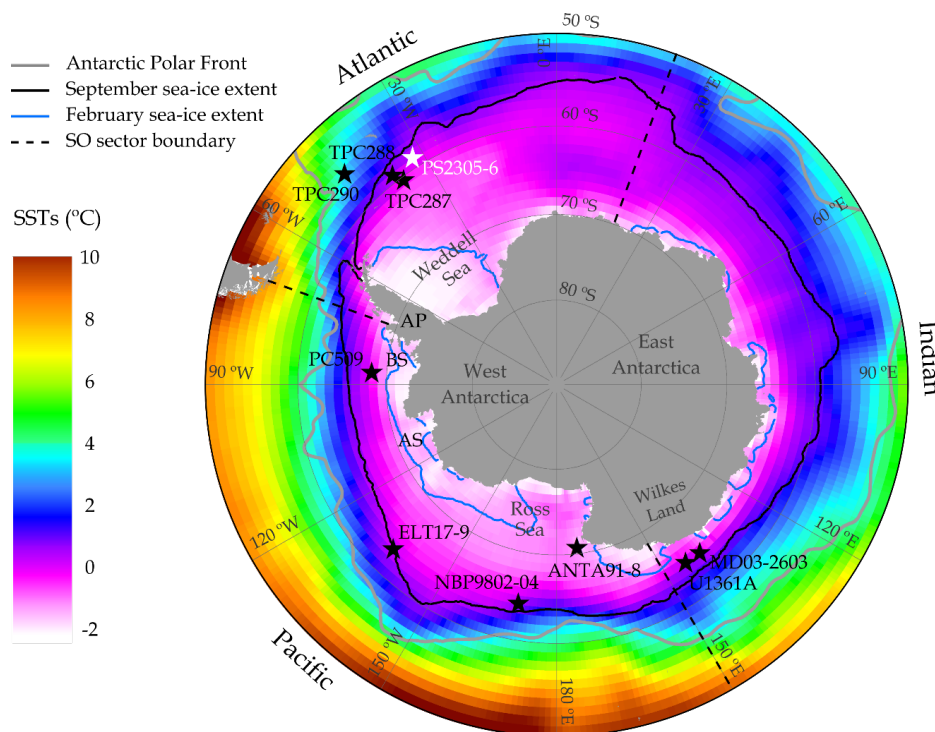
Figure 1: Map of core locations (black stars – this study, white star – Bianchi and Gersonde (2002)) with the modern (1981-2010) mean annual SSTs (COBE-SST2 dataset provided by the NOAA PSL, Boulder, Colorado, USA (https://psl.noaa.gov/)) and modern (1981-2010) median September and February sea-ice extents (data from Fetterer et al. (2017)). The black solid line is the September sea-ice extent (15 % cover) and the blue solid line is the February sea-ice extent (15 % cover). The grey solid line is the position of the modern Antarctic Polar Front (Trathan et al., 2000). The black dashed lines mark the boundaries between the three SO sectors (Atlantic, Indian and Pacific). AP – Antarctic Peninsula, BS – Bellingshausen Sea, AS – Amundsen Sea.

67   Diatoms preserved in SO marine sediments have been used for over 40 years to reconstruct past

68   changes in Antarctic sea-ice extent and sea-surface temperatures (SSTs) (Armand and Leventer, 2010;

69   Burckle et al., 1982; Thomas et al., 2019) due to the close relationship between their biogeographic

70   distribution patterns and surface water environmental conditions (Armand et al., 2005; Crosta et al.,

71   2005; Esper et al., 2010; Gersonde and Zielinski, 2000; Romero et al., 2005; Zielinski and Gersonde,

72   1997). Several previous studies have used model simulations, alongside limited data constraints from

73   marine sediment cores, to reconstruct SO WSIE and SSTs during MIS 5e (Capron et al., 2017; Holloway

74   et al., 2017; Holloway et al., 2018). However, there are currently no marine core records located far

75   enough south to constrain the predicted WSIE during MIS 5e (Chadwick et al., 2020; Holloway et al.,

76   2017). Due to chronological uncertainties in SO proxy records (Govin et al., 2015), previous studies

77   have assumed the minimum WSIE occurred synchronously around Antarctica and was coincident with

78   peak atmospheric temperatures in Antarctic ice cores at 128 ka (Holloway et al., 2017).

79   This study presents new reconstructions of SO winter sea ice (WSI) during MIS 5e from the diatom

80   assemblages preserved in nine marine sediment cores located south of 55 °S and south of the modern

81   Antarctic Polar Front (Figure 1). Quantitative and qualitative reconstructions of WSIE in the three SO

82   sectors; the Atlantic sector (70 °W – 20 °E), the Indian sector (20 °E – 150 °E) and the Pacific sector

83   (150 °E – 70 °W), are compared to answer the following questions:

84   -   Did the minimum WSIE occur synchronously throughout the SO during MIS 5e?

85   -   Was the WSIE minimum concurrent with the peak Antarctic air temperatures at 128 ka?

86   -   Were the patterns in MIS 5e sea-ice change consistent between SO sectors?

2. Materials and methods

2.1. Core sites

89   The nine sediment cores used in this study are shown in Figure 1 alongside modern SSTs and sea-ice

90   extents. Details for each core are listed in Table 1. These cores were chosen as they contain >20 cm of

Core	Latitude (°), Longitude (°)	Water depth (m)	Cruise, Year	Ship	Core length (cm)
TPC290	-55.55, -45.02	3826	JR48, 2000	*RRS James Clark Ross*	1179*
TPC288	-59.14, -37.96	2864	JR48, 2000	*RRS James Clark Ross*	940*
TPC287	-60.31, -36.65	1998	JR48, 2000	*RRS James Clark Ross*	615*
MD03-2603	-64.28, 139.38	3320	MD130, 2003	*R/V Marion DuFresne II*	3033
U1361A	-64.41, 143.89	3459	IODP Exp. 318, 2010	*R/V JOIDES Resolution*	38800
ELT17-9	-63.08, -135.12	4935	ELT17, 1965	*R/V Eltanin*	2018
NBP9802-04	-64.20, -170.08	2696	PA9802, 1998	*R/V Nathaniel B. Palmer*	740
PC509	-68.31, -86.03	3559	JR179, 2008	*RRS James Clark Ross*	989
ANTA91-8	-70.78, 172.83	2383	ANTA91, 1990	*R/V Cariboo*	511

Table 1: Details of the location and recovery information for the nine marine sediment cores analysed in this study. Cores are ordered by sector (Atlantic-Indian-Pacific) and then latitude. * For each of the three TPC cores (TPC290, TPC288 and TPC287), the trigger core (TC) and piston core (PC) were spliced together to produce a composite record.

91   diatom rich MIS 5e sediments and are located further south than almost all existing MIS 5e sea ice

92   records (Chadwick et al., 2020).

93   *2.2.   Diatom counts*

94   For the diatom assemblage data, microscope slides were produced using a method adapted from

95   Scherer (1994). Samples of 7-28 mg were exposed to 10% Hydrochloric acid to remove any carbonate,

96   30% Hydrogen peroxide to break down organic material and a 4% Sodium Hexametaphosphate

97   solution to promote disaggregation and placed in a warm water bath for a minimum of 12 hours. The

98   material was homogenised, transferred into a ~10 cm water column and allowed to settle randomly

99   onto coverslips over a minimum of 4 hours. The water was drained away and coverslips were mounted

100   on microscope slides with Norland Optical Adhesive (NOA 61). Slides were examined using a light

101   microscope (Olympus BH-2 at x1000 magnification) and a minimum of 300 diatom valves were

102   counted for each sample.

103   The combined relative abundance of *Fragilariopsis curta* and *F. cylindrus* (FCC) is used as a qualitative

104   indicator of WSI presence (Gersonde and Zielinski, 2000), with abundances >3 % associated with

105   locations south of the mean WSI edge, abundances 1-3 % found between the mean and maximum

106   WSI edge and abundances <1 % indicative of conditions north of the maximum WSI edge (Gersonde

107   et al., 2005; Gersonde and Zielinski, 2000).

108   *2.3.   Modern Analog Technique (MAT)*

109   September sea-ice concentrations (SIC) and SSSTs (January to March) are estimated by applying the

110   MAT transfer function, detailed in Crosta et al. (2020) , to the MIS 5e diatom assemblages. The MAT

111   compares the relative abundances of 33 diatom species in each MIS 5e sample to the abundances of

112   the same species in a modern reference dataset composed of 257 surface sediment samples (modern

113   analogs) from the SO. Modern conditions for each surface sediment sample are interpolated on a 1° x

114   1° grid, with SSSTs from the World Ocean Atlas 2013 (Locarnini et al., 2013) and September SIC from

115   the numerical atlas of Schweitzer (1995). The MAT was implemented using the "bioindic" R-package

116   (Guiot and de Vernal, 2011), with chord distance used to select the 5 most similar modern analogs to

117   each MIS 5e assemblage. A cut-off threshold, above which any analogs are deemed too dissimilar to

118   the MIS 5e sample, is fixed as the first quartile of random distances determined by a Monte Carlo

119   simulation of the reference dataset (Simpson, 2007).

120   Quantitative estimates of September SIC and SSSTs are produced for each MIS 5e sample from a

121   distance-weighted average of the climate values associated with the selected analogs. The

122   reconstructed SSSTs have a Root Mean Square Error of Prediction (RMSEP) of 1.09 °C and an R^2 of

123   0.96, and the reconstructed September SIC have a RMSEP of 9 % and an R^2 of 0.93. It is also possible

124   to get no-analog conditions, where none of the reference surface sediment samples are similar

125   enough to a MIS 5e sample, and it is therefore not possible to reconstruct September SIC and SSST for

126   this MIS 5e sample. The reconstructed September SIC and SSST for each MIS 5e sample only use

127   analogs below the dissimilarity threshold and therefore could be reconstructed from less than 5

128   analogs in some samples.

Core	SO sector	Chronology for MIS 5e	Chronological uncertainty (ka)
TPC290	Atlantic	Correlating MS from TPC290 to EDC ice core dust record combined with *C. davisiana* abundances (Pugh et al., 2009)*	± 2.58
TPC288	Atlantic	Correlating MS from TPC288 to EDC ice core dust record combined with *C. davisiana* abundances (Pugh et al., 2009)	± 2.59-2.64
TPC287	Atlantic	Correlating MS from TPC287 to MS in core TPC288 (Chadwick et al., *in review*)	± 2.57-2.65
MD03-2603	Indian	Correlating Ba/Al and Ba/Ti ratios from MD03-2603 to LR04 benthic oxygen isotope stack combined with diatom biostratigraphy (Presti et al., 2011)	± 2.55-2.56
U1361A	Indian	Correlating Ba/Al ratios and lithological changes to the LR04 benthic oxygen isotope stack combined with LOD *H. karstenii* (Wilson et al., 2018)	± 2.62-2.70
ELT17-9	Pacific	Combined abundance stratigraphies of *E. antarctica* and *C. davisiana* on SPECMAP age scale (Chase et al., 2003)	± 2.51
NBP9802-04	Pacific	Correlating MS from NBP9802-04 to EDC ice core dust record combined with LOD *H. karstenii* (Williams, 2017)	± 2.68
PC509	Pacific	Correlating wet bulk density (= proxy mirroring biogenic opal content) from PC509 to the LR04 benthic oxygen isotope stack (Chadwick et al., *in review*)	± 2.59-2.65
ANTA91-8	Pacific	Correlating MS from ANTA91-8 to the LR04 benthic oxygen isotope stack combined with LCO *Rouxia* spp. (this study; Figure 2)	± 2.60

Table 2: Summary of the location and chronologies for the nine sediment cores analysed in this study. Cores are ordered by sector (Atlantic-Indian-Pacific) and then latitude. LOD: Last Occurrence datum, LCO: Last Common Occurrence *For core TPC290 the chronology has been slightly adjusted from the published record of Pugh et al. (2009) by shifting the Termination II tiepoint to better align the magnetic susceptibility (MS) record with the dust record of the EPICA Dome C (EDC) ice core in East Antarctica (Chadwick et al. *in review*).

129   **3. Age models**

130   *3.1. Published chronologies*

131   Eight of the sediment cores presented in this study have previously published age models, summarised

132   in Table 2. Cores TPC290, TPC288, TPC287 and NBP9802-04 are published on the EDC3 chronology,

133   cores MD03-2603, U1361A and PC509 are published on the LR04 chronology and core ELT17-9 is

134   published on the SPECMAP chronology. To allow for consistent comparison of timings between cores,

135   all cores are translated across onto the AICC2012 chronology (Bazin et al., 2013; Veres et al., 2013)

136   using the alignment strategy in Govin et al. (2012) and the conversion tables in Lisiecki and Raymo

137   (2005) and Parrenin et al. (2013).

138   Chronological uncertainties for the MIS 5e ages of samples in this study (Table 2) vary between 2.5

139   and 2.7 ka. The AICC2012 chronology has an uncertainty of ±1.5 ka during MIS 5e, with an additional

140   uncertainty of ±1 ka arising from the translation between chronologies (Capron et al., 2014). Each core

141   sample comprises a 0.5 cm thick slice of sediment, and therefore additional age uncertainty due to

142   integrating over the corresponding time interval in each core needs to be taken into account (see

143   Table 2).

144   *3.2. ANTA91-8 chronology*

145   The chronology for core ANTA91-8 was constructed by aligning the magnetic susceptibility (MS) to the

146   LR04 benthic foraminifera δ^{18}O stack (Lisiecki and Raymo, 2005) using the AnalySeries software

147   (Paillard et al., 1996). Increased supply of terrigenous glacigenic detritus from the Antarctic continent

148   to its margin and increased dust input from Patagonia and Australia to the pelagic SO during glacial

149   periods resulted in higher MS values during glacial periods than interglacial periods (Bareille et al.,

150   1994; Pugh et al., 2009; Walter et al., 2000). Tie points were selected in the MS record at the

151   boundaries of MIS stages and sub-stages (Figure 2 & Table 3). Ages for the MIS 5 sub-stage boundaries

ANTA91-8 depth (mbsf)	LR04 Age (ka)	MIS stage/sub-stage boundary
0.65	14	1-2
2.09	71	4-5a
2.39	83	5a-b
2.55	105	5c-d
2.65	116	5d-e
3.05	131.5	5e-6
3.17	136	-

Table 3: Tiepoints for ANTA91-8 chronology. The MS record for ANTA91-8 is aligned to the LR04 benthic stack using the AnalySeries software (Paillard et al., 1996).

Figure 2: Alignment between the MS from core ANTA91-8 (red) and the LR04 benthic δ^{18}O stack (black) using the AnalySeries software (Paillard et al., 1996). Blue squares and connecting lines mark the tiepoints between records.
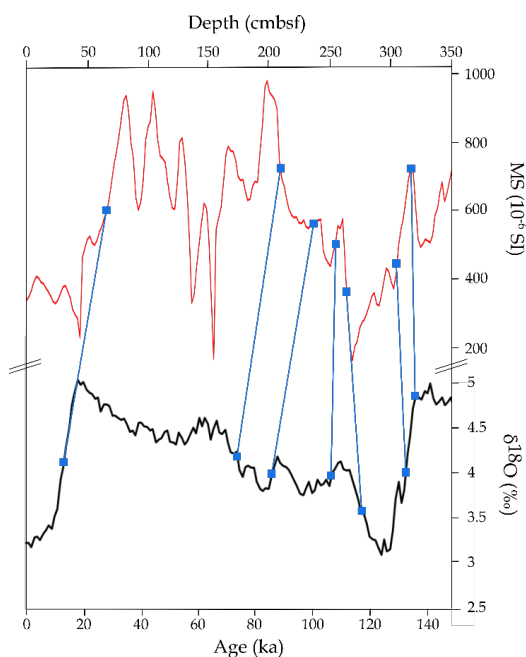
152   are from Govin et al. (2009), and the ages are translated from the LR04 chronology onto the AICC2012

153   chronology.

154   The chronology for core ANTA91-8 presented in this study differs from chronologies previously

155   published by Ceccaroni et al. (1998) and Brambati et al. (2002), who – on the basis of [230]Thorium

156   measurements, subsequently adjusted by matching maxima in palaeo-productivity proxies to peak

157   interglacials – placed MIS 5e ~50 cm higher than in our age model (Supplementary Figure 1). Our new

158   chronology assigns the broad MS minimum from 2.65-3.05 mbsf, which comprises a peak in organic

159   carbon content (Ceccaroni et al., 1998), to MIS 5e. In contrast, both the Ceccaroni et al. (1998) and

160   Brambati et al. (2002) age models placed this MS minimum within MIS 6 (Supplementary Figure 1),

161   resulting in inexplicably high accumulation rates of productivity proxies during this glacial period

162   (Ceccaroni et al., 1998). Our new chronology is corroborated by the diatom group *Rouxia* spp., which

163   occurs in abundances <1 % in ANTA91-8 samples between 2.72 and 3.14 mbsf (Chadwick and Allen,

164   2021a). If the samples in this depth interval were deposited during MIS 6, as suggested by the

165   Ceccaroni et al. (1998) and Brambati et al. (2002) age models, then the *Rouxia* spp. abundances should

166   be >1 % (Zielinski et al., 2002).

167   **4. Results**

168   The September SIC values, reconstructed using the MAT, and the FCC relative abundances are

169   presented for the 132-120 ka interval in all nine sediment cores (Figure 3). This interval is chosen to

170   capture the sea-ice signature from both the end of glacial Termination II and during 'peak' MIS 5e.

171   SSST data, also reconstructed using MAT, is presented over the same time interval alongside the

172   cumulative relative abundance of the eight tropical/subtropical diatom species and groups according

173   to Romero et al. (2005).

174   *4.1. Sea ice*

175   In the Atlantic sector, the three cores (TPC290, TPC288 and TPC287) display a N-S increasing trend in

176   mean FCC relative abundances (2.1 ± 0.7 %, 3.1 ± 2.2 % and 4.7 ± 3.6 %) and Sept. SICs (19 ± 17 %, 25

177   ± 18 % and 33 ± 20 %). All three cores have low FCC relative abundances (1.2 ± 0.5 %) and Sept. SICs

178   (8.8 ± 4.6 %) during the 131-130 ka interval, with cores TPC288 and TPC287 both reaching their

179   minimum MIS 5e Sept. SIC and FCC values at this time (Figure 3). Following this interval of low Sept.

180   SIC and FCC values, all three cores show an increase to their maximum Sept. SICs (58 ± 5 %) and FCC

181   relative abundances (9 ± 5 %) at 127-126 ka (Figure 3). After 126 ± 2.6 ka core TPC290 displays a

182   gradual decline in both FCC relative abundance and Sept. SIC to minimum values at 121-120 ka (Figure

183   3). In contrast, core TPC287 maintains high Sept. SICs (51 ± 3 %, multiple samples) throughout the 126-

184   120 ka period as well as high (6.2 ± 1.8 %, multiple samples) FCC relative abundances, although they

185   are lower than the 126 ± 2.6 ka peak of ~15 % (single sample) (Figure 3). Core TPC288 maintains,

186   relative to the ~130 ± 2.6 ka minimum and ~126 ± 2.6 ka maximum, intermediate FCC (2.9 ± 0.6 %,

187   multiple samples) and Sept. SIC (22 ± 15 %, multiple samples) values throughout the 126-120 ka

188   interval, however the Sept. SICs are much more variable than in TPC287 (Figure 3).
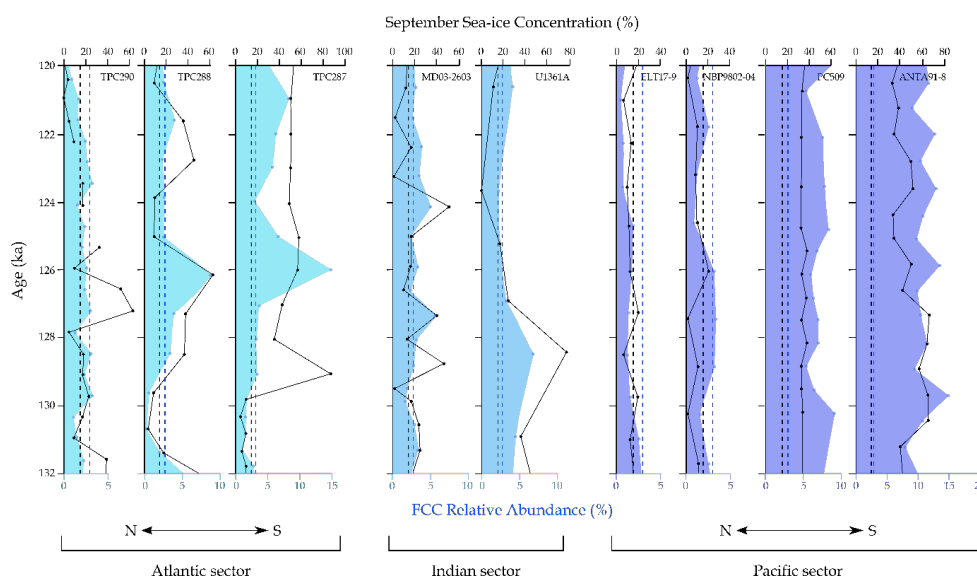
189

Figure 3: Downcore September SICs, determined using the MAT, and FCC relative abundances for the 132-120 ka interval in nine marine sediment cores. The blue shading indicates the FCC relative abundance, with the colour saturation varying between SO sectors. The solid black lines indicate the September SICs with the gaps in the TPC290 record caused by two samples being too dissimilar from all modern reference samples, so that the latter cannot be considered as analogs. Dashed lines mark the mean WSIE thresholds of 3 % FCC abundance (blue lines) and 15 % Sept. SIC (black lines). Within each SO sector cores are arranged from north to south.

190   All three Atlantic sector cores (TPC290, TPC288 and TPC287) have a strong match (p = 0.05, p <0.01

191   and p <0.01 respectively) between the FCC and Sept. SIC variations, with the notable exception of the

192   TPC287 sample at ~129 ± 2.6 ka which has a very high Sept. SIC (86 %) but a relatively low FCC relative

193   abundance (3.4 %). The only pronounced difference between the diatom species assemblage in this

194   sample compared to neighbouring depths is a substantially higher relative abundance of *F. separanda*

195   (Chadwick and Allen, 2021f), a species known to achieve highest abundances in modern sediments

196   overlain by winter SICs above 60 % (Armand et al., 2005). There was also only a single modern analog

197   identified for this sample and so it is likely that the high *F. separanda* relative abundance (~9 %) has

198   biased the MAT reconstruction towards colder conditions with a greater SIC than the conditions

199   reflected by the rest of the diatom species assemblage for that sample. Thus, the reconstructed Sept.

200 SIC for this sample is disregarded from the analysis. There are two MIS 5e samples in TPC290 (at 124.7

201 ± 2.6 ka and 122.8 ± 2.6 ka) for which none of the reference surface sediment samples were below

202 the dissimilarity threshold (see section 2.3 for details) and thus no MAT estimate of Sept. SIC (or SSST)

203 is given for those samples.

204 The two Indian sector cores (MD03-2603 and U1361A) have similar average MIS 5e FCC relative

205 abundances (3.2 ± 1 % and 3.9 ± 1.5 %) to each other but the average Sept. SIC (19 ± 15 % and 27 ± 25

206 %) is nearly 10 % higher in U1361A. However, the MIS 5e variability in Sept. SIC within each core is

207 greater than this difference between the two cores. Core MD03-2603 has three Sept. SIC maxima of

208 >40 % (single samples) during MIS 5e, at 124.1 ± 2.6 ka, 127.3 ± 2.6 ka and 128.8 ± 2.6 ka, as well as

209 three minima of <5 % (single samples) at 121.5 ± 2.6 ka, 123.3 ± 2.6 ka and 129.5 ± 2.6 ka (Figure 3).

210 Contrastingly, the nearby core U1361A (Figure 1) has a maximum in MIS 5e Sept. SIC (76.4 %, single

211 sample) at 128.4 ± 2.7 ka and a minimum (0 %, single sample) at 123.7 ± 2.7 ka (Figure 3). Together

212 these two records suggest that the greatest MIS 5e Sept. SICs in the Indian sector occurred during the

213 129-127 ka interval and the minimum was at 123.5-121 ka (Figure 3).

214 Unlike the Atlantic and Indian sectors, the four cores from the Pacific sector (ELT17-9, NBP9802-04,

215 PC509 and ANTA91-8) have low variability in their FCC relative abundances (1.4 ± 0.6 %, 2.3 ± 1 %, 5.8

216 ± 0.9 % and 11 ± 1.9 %) and Sept. SICs (13 ± 4 %, 8.4 ± 5.7 %, 34 ± 2 % and 48 ± 11 %) throughout MIS

217 5e, with no pronounced maxima or minima (Figure 3). The northernmost Pacific sector core ELT17-9

218 has the lowest average MIS 5e FCC relative abundance (1.4 ± 0.6 %) but the more southerly core

219 NBP9802-04 has the lowest average MIS 5e Sept. SIC (8.4 ± 5.7 %). The two most southerly Pacific

220 sector cores (PC509 and ANTA91-8) have the highest average MIS 5e Sept. SICs and FCC relative

221 abundances of all the cores analysed for this study.

222   *4.2. Sea-surface temperatures*

223 For the Atlantic sector cores the average MIS 5e SSSTs (3.2 ± 1.9 °C, 2.7 ± 1.6 °C and 2.2 ± 1.5 °C) show

224 an inverse trend to Sept. SICs with higher values in more northerly cores. Both TPC288 and TPC287

225 have their highest MIS 5e SSSTs during the 131-129 ka interval (5 °C and 4.3 °C, respectively, multiple

226 samples) followed by a SSST minimum at ~126 ± 2.6 ka (0.1 °C and 0.6 °C, respectively, single samples)

227 (Figure 4). In contrast, the warmest MIS 5e SSSTs for TPC290 occur in the youngest part of the record,

228 with an average of 6 °C in the 122-120 ka period (Figure 4). The relative abundance of subtropical

229 diatoms in core TPC290 shows a good consistency (p <0.01, R^2 = 0.51) with the SSST pattern during

230 MIS 5e, with the highest relative abundances (1.6 ± 0.8 %, multiple samples) after 126 ± 2.6 ka (Figure

231 4). In the southernmost Atlantic sector core TPC287 there is a very poor match between MIS 5e SSSTs

232 and subtropical diatom relative abundances (p = 0.3, R^2 = 0.11). This lack of correlation is likely due to

233   the scarcity of subtropical diatoms at this site throughout MIS 5e, as can be seen in modern surface

234   sediments (Chadwick, 2020), and thus a single valve can create a relative abundance peak that may

235   be largely unrelated to the SSST trends.
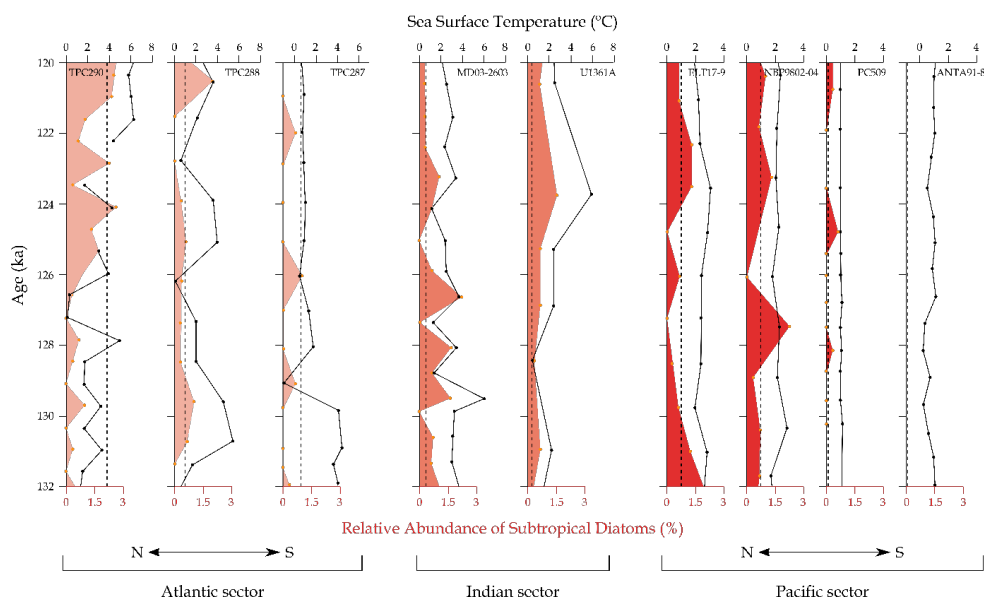
Figure 4: Downcore summer (January to March) SSTs, determined using the MAT, and the relative abundance of all tropical/subtropical diatom species (Romero et al., 2005) for the 132-120 ka interval in nine marine sediment cores. The red shading indicates the relative abundance of subtropical diatom species, with the colour saturation varying between SO sectors. The solid black lines indicate the SSSTs with the gaps in the TPC290 record caused by two samples being too dissimilar from all modern reference samples, so that the latter cannot be considered as analogs. Black dashed lines mark the modern (Jan-Mar, 1980-2019) SSSTs at each core site (Hersbach et al., 2019). Within each SO sector cores are arranged from north to south.

237   The Indian sector cores have similar average SSSTs (2.8 ± 1.1 °C and 2.4 ± 1.7 °C). However, unlike for

238   the Sept. SICs (Figure 3), the MIS 5e SSST minima and maxima in cores MD03-2603 and U1361A occur

239   at different times (Figure 4). SSSTs in core U1361A fall to a minimum of 0.7 °C (single sample) at ~128

240   ± 2.7 ka before rising to a maximum of 5.9 °C (single sample) at ~124 ± 2.7 ka. In contrast, SSSTs in

241   core MD03-2603 reach an early peak of 5.9 °C (single sample) at ~129.5 ± 2.6 ka and have minima of

242   ~1 °C (single samples) at 124.1 ± 2.6 ka, 127.3 ± 2.6 ka and 128.8 ± 2.6 ka (Figure 4). Both MD03-2603

243   and U1361A show a strong coherence between the MIS 5e SSSTs and the subtropical diatom

244   abundance (p = 0.02, R^2 = 0.34 and p <0.01, R^2 = 0.98 respectively).

245   In the Pacific sector cores, SSSTs are largely consistent throughout MIS 5e, with averages of 2.5 ± 0.3

246   %, 2.2 ± 0.3 %, 1.03 ± 0.03 % and 0.8 ± 0.3 % (Figure 4). Although there is very little variation in MIS 5e

247   SSSTs in all four records, both core NBP9802-04 and core PC509 reveal maximum SSSTs (2.8 °C and 1.1

248   °C, respectively, single samples) at ~130 ± 2.7 ka (Figure 4). None of the Pacific sector cores show a

249   strong match between MIS 5e SSSTs and the relative abundance of subtropical diatom species. For

250   the more southerly core PC509 this poor correlation (p = 0.65, R^2 = 0.02) is likely caused by the same

251   scarcity of subtropical diatoms as for core TPC287 in the Atlantic sector.

252   **5. Discussion**

253   Both the Sept. SICs and FCC relative abundances indicate substantial differences in the pattern of MIS

254   5e WSIE change between the three SO sectors, most notably between the Atlantic and Pacific sectors.

255   In all three Atlantic sector records, the FCC relative abundances and Sept. SICs indicate year-round

256   open marine conditions and thus a poleward contraction of the mean WSIE (FCC <3 % (Gersonde and

257   Zielinski, 2000) and Sept. SIC <15 % (Zwally et al., 2002)) during the 131-130 ka interval. This minimum

258   is succeeded by a re-expansion of sea ice to a maximum extent in the 127-126 ka interval when all

259   three core sites were covered by WSI. An early minimum in MIS 5e WSIE succeeded by a maximum ~4

260   ka later is consistent with the FCC relative abundance in nearby core PS2305-6 (Figure 1; 58.72 °S,

261   33.04 °W) (Bianchi and Gersonde, 2002; Chadwick et al., 2020). The MIS 5e WSIE maximum in the

262   Atlantic sector records coincides, within chronological uncertainty, with higher global sea level (Kopp

263   et al., 2013) and evidence for increased meltwater flux in the Weddell Sea (Chadwick et al., *in review*),

264   which both indicate substantial mass loss from the Antarctic ice sheets, consistent with findings of

265   major ice loss in the Weddell Sea sector during MIS 5e (Turney et al., 2020). Higher glacial meltwater

266   fluxes associated with increased ice-sheet loss could therefore be a major driver of the WSIE expansion

267   in the Atlantic sector records as less saline surface waters freeze more easily (Bintanja et al., 2013;

268   Merino et al., 2018). The peak in FCC abundance in core TPC287 at 126 ± 2.6 ka is primarily a peak in

269   the abundance of *F. cylindrus* (Chadwick and Allen, 2021f) which is affiliated with sea-ice melt and

270   strong surface stratification (Cremer et al., 2003; von Quillfeldt, 2004) and further supports an

271   increased glacial meltwater signal at this time.

272   The discrepancy between Sept. SICs and FCC relative abundances at ~127 ± 2.6 ka in core TPC290

273   (Figure 3) is likely due to increased *Chaetoceros* resting spore (rs.) abundance at this time (Chadwick

274   and Allen, 2021h). For core TPC290, there is a scarcity of modern analogs from the Scotia Sea region

275   (Gersonde et al., 2005) and thus, the high *Chaetoceros* rs. abundances in MIS 5e samples are

276   associated with modern analogs from sites along the Antarctic Peninsula, where SICs are greater than

277   in the Scotia Sea.

278   In the Indian sector, core MD03-2603 has an average MIS 5e Sept. SIC (25 ± 18 %) and FCC relative

279   abundance (3.2 ± 1 %) indicative of a location just south of the mean WSIE (Figures 3 & 5) but with
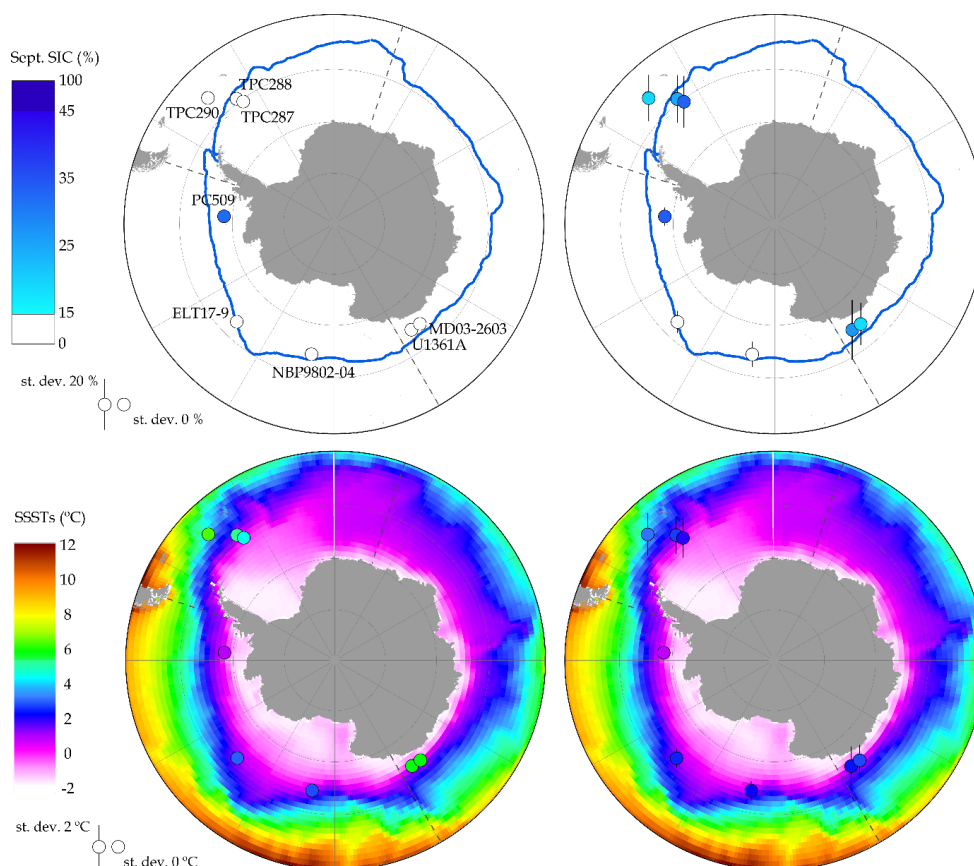
Figure 5: Maps of MIS 5e SSSTs and Sept. SICs for the nine core sites compared with the modern conditions. On all maps the SO sector boundaries are marked with dashed lines. **Top left:** Minimum MIS 5e Sept. SIC for each core site (coloured circles) compared to the modern (1981-2010) 15 % September sea-ice extent (blue line) (Fetterer et al., 2017). **Top right:** Average MIS 5e Sept. SICs (coloured circles) and standard deviations (vertical bars) at each core site compared to the modern (1981-2010) 15 % September sea-ice extent (blue line) (Fetterer et al., 2017). **Bottom left:** Maximum MIS 5e SSSTs for each core site (coloured circles) compared to modern (Jan-Mar, 1980-2019) SSSTs (Hersbach et al., 2019). **Bottom right:** Average MIS 5e SSSTs (coloured circles) and standard deviations (vertical bars) for each core site compared to modern (Jan-Mar, 1980-2019) SSSTs (Hersbach et al., 2019). Core data are given in Supplementary Table 1.

280   multiple maxima and minima contributing to the high variability. MIS 5e Sept. SICs and FCC relative

281   abundances in the nearby core U1361A indicate that it was located within the seasonal sea-ice zone

282   from 132-126 ka before the mean WSIE retreated to the south of this location (Figure 3 &

283   Supplementary Figure 2). The different patterns in MIS 5e Sept. SIC and SSSTs between cores MD03-

284   2603 and U1361A are likely due to the different age resolution of the samples, with two of the Sept.

285   SIC maxima in MD03-2603 occurring in the 129-127 ka interval coincident with the U1361A Sept. SIC

286   maximum, and likewise, two of the Sept. SIC minima in MD03-2603 occurring in the 124-121 ka period

287 concurrent with the minimum Sept. SIC in core U1361A (Figure 3). The different age resolution of

288 samples in MD03-2603 and U1361A is primarily due to the lower sedimentation rate (Table 2) at site

289 U1361A, and thus a sample from this core spans more time than in core MD03-2603.

290 None of the Pacific sector cores show pronounced minima or maxima in their MIS 5e FCC and Sept.

291 SIC records (Figure 3), indicating a less variable WSIE in this sector compared to the Atlantic and Indian

292 sectors (Figure 3). The Pacific sector cores PC509 and ANTA91-8 are also the only cores in this study

293 which are covered by WSI for the entirety of MIS 5e (Figure 3 & 5). The position of these cores south

294 of the mean WSIE throughout MIS 5e is significant as they are the first published marine records from

295 within the seasonal sea ice zone and able to constrain the poleward limit of the MIS 5e minimum WSIE

296 (Chadwick et al., 2020). Cores ELT17-9 and NBP9802-04 are the only records in this study with average

297 MIS 5e Sept. SICs <15 % (Figure 5), indicating they were located north of the mean WSIE for the

298 majority of the 132-120 ka period, with core ELT17-9 having been located closer to the MIS 5e mean

299 WSIE. The FCC relative abundances for cores ELT17-9 and NBP9802-04 also indicate that both were

300 located on average north of the mean WSIE during MIS 5e (Figure 3) but suggest that core NBP9802-

301 04 was located closer to the MIS 5e mean WSIE.

302 The reconstructed MIS 5e Sept. SICs for site ELT17-9 are higher than for site NBP9802-04 (Figure 3)

303 which is likely related to the higher abundance of *Chaetoceros* rs. in core ELT17-9 when compared to

304 core NBP9802-04 (Chadwick and Allen, 2021b, d). The *Chaetoceros* rs. group is associated with both

305 WSI (Armand et al., 2005) and meltwater stratification (Crosta et al., 1997), and it reached high

306 abundances in the Ross Sea during past interglacials (Kim et al., 2020). The high *Chaetoceros* rs.

307 abundance in core ELT17-9 during MIS 5e could therefore indicate an north-eastward shift of the Ross

308 Sea gyre from its modern day position (Dotto et al., 2018) and an accompanying displacement of

309 meltwater circulation (Merino et al., 2016) and the WSI edge in the Pacific sector.

310 The average MIS 5e SSSTs in the nine cores are ~1-2 °C warmer than the modern SSSTs (Figure 5),

311 consistent with the SST anomalies presented in Chadwick et al. (2020) and Capron et al. (2014).

312 However, the SSST records in the Atlantic and Indian sectors have large variability with maximum

313 SSSTs that are 2-4 °C higher than the MIS 5e average SSSTs (Figure 5). Maximum MIS 5e SSSTs in the

314 Atlantic and Indian sectors were therefore ~3-5 °C warmer than modern SSSTs (Figure 5), which is a

315 much larger SSST anomaly than the Antarctic Zone (south of the Antarctic Polar Front) records

316 presented in Chadwick et al. (2020), and marks a ~5 degrees latitude poleward shift in SSST isotherms

317 relative to the present. Unlike the Atlantic and Indian sectors, the Pacific sector core records indicate

318 low variability in MIS 5e SSSTs with peak values 0-2 °C warmer than present (Figure 5) marking a

319 poleward shift in SSST isotherms of <3 degrees latitude.

320 Within their chronological uncertainties (Table 2), cores TPC288, TPC287, MD03-2603, ELT17-9,

321 NBP9802-04 and PC509 all reach minimum MIS 5e Sept. SICs synchronously (Supplementary Table 1)

322 and coincident with the peak in Antarctic air temperatures and minimum in EPICA Dome C (EDC) sea-

323 salt sodium flux (Na_{ss}) at ~128 ± 1.5 ka (Holloway et al., 2017; Wolff et al., 2006). The two Indian sector

324 core records reach a minimum MIS 5e WSIE (and maximum SSST in core U1361A) ~4.5 ka after the

325 Na_{ss} minimum in Antarctic ice cores, outside of the combined chronological uncertainties of the

326 sediment cores (Table 2) and AICC2012 ice core chronology (Bazin et al., 2013). Although the duration

327 of the SSST maximum, and accompanying WSIE minimum, in core MD03-2603 is short, it occurs within

328 chronological error of the maximum air temperatures in Antarctic ice cores (Figures 3 & 4).

329 Satellite era trends in Antarctic winter SIC (Hobbs et al., 2016) are largely consistent with the patterns

330 observed during MIS 5e. Northern Weddell Sea winter SIC has declined by 5-10 % per decade in the

331 satellite era (Hobbs et al., 2016) indicating a sensitivity to warming consistent with the early retreat

332 of MIS 5e sea ice in this region. Similarly, winter SICs in the Pacific sector have remained stable, or

333 even slightly increased, during the satellite era (Hobbs et al., 2016) which is in agreement with the

334 stability of the Pacific sector WSIE throughout MIS 5e. In recent decades, Bellingshausen Sea summer

335 sea ice has decreased, whilst WSIE has stayed stable (Hobbs et al., 2016; Parkinson, 2019). The MIS 5e

336 Sept. SICs and SSSTs (as a proxy for summer sea ice) imply that the MIS 5e WSIE in the Bellingshausen

337 Sea is similar to the modern but the summer sea-ice extent was reduced. The western Ross Sea is a

338 region in which the modern and MIS 5e trends differ, with recent winter SIC increases of 10-15 % per

339 decade contrasting with the MIS 5e WSIE reduction observed at site NBP9802-04.

340 ## 6. Conclusions & wider implications

341 During MIS 5e the three SO sectors display heterogeneous responses in WSIE and SSSTs, which may

342 guide our predictions of the impact of future warming on the Antarctic region. The prominent early

343 (131-130 ka) minimum in WSIE and coinciding maximum in SSSTs for the two southerly Atlantic sector

344 cores (TPC288 and TPC287, Figure 3) is associated with a mean WSI edge located at least 3-5 ° south

345 of its modern position. This substantial reduction in WSIE and seasonal sea-ice cover would have

346 reduced brine rejection and likely decreased the rates of deep and bottom water formation in the

347 Weddell Sea, causing a warming of the abyssal waters (Bouttes et al., 2010; Marzocchi and Jansen,

348 2019). Deep water warming would have promoted the basal melting and retreat of Weddell Sea ice

349 shelves and marine terminating ice streams and caused substantial Antarctic ice sheet mass loss

350 (Hellmer et al., 2012; Rignot et al., 2019; Wahlin et al., 2021). We hypothesise that substantial mass

351 loss from the Weddell Sea sector drove the Atlantic sector WSI resurgence at ~126 ± 2.6 ka and

352 contributed to the global sea-level rise at this time (Kopp et al., 2013; Sime et al., 2019).

353   Variations in the WSIE and SSST records between the Indian sector cores MD03-2603 and U1361A are

354   due to the differences in sampling resolution, with the MD03-2603 record indicating multiple

355   relatively short duration WSIE and SSST oscillations during MIS 5e. The U1361A record seems to

356   present an averaged signal of these oscillations with a greater frequency of warm periods with

357   reduced WSIE after 125 ± 2.7 ka. Along the modern Wilkes Land margin the Antarctic Circumpolar

358   Current (ACC) flows much closer to the continent than in other regions (Tamsitt et al., 2017) and the

359   MIS 5e record in core MD03-2603 could therefore suggest multiple intervals when the ACC was

360   displaced to the south of its modern position. A more southerly ACC in this region would have caused

361   a poleward shift in precipitation fields and resulted in drier conditions across Southern Australia (Liu

362   and Curry, 2010; Saunders et al., 2012), a trend that can already be observed under a modern warming

363   climate (CSIRO, 2018). A southerly shift of the ACC would also increase the advection of warmer

364   Circumpolar Deep Water onto the Antarctic continental shelf (Fogwill et al., 2014), promoting periods

365   of high basal melting and ice sheet retreat in Wilkes Land during MIS 5e, as supported by Wilson et al.

366   (2018).

367   In contrast to the Atlantic and Indian sectors, the Pacific sector records indicate a more stable WSIE

368   throughout MIS 5e. The MIS 5e Sept. SIC records of cores ELT17-9 and NBP9802-04 indicate a

369   poleward shift in the mean WSI edge by at least 2 ° of latitude relative to the modern. The PC509

370   record indicates a southerly shift in the mean WSI edge by <2 ° latitude, highlighting a seemingly

371   greater resilience of sea ice in the Bellingshausen Sea with the WSI edge having remained north of 68

372   °S throughout MIS 5e. In the modern Pacific sector the WSIE is strongly constrained by the southern

373   extent of the ACC and the shape of the Ross Sea gyre (Benz et al., 2016; Nghiem et al., 2016). An

374   uneven poleward constriction of the ACC across the Pacific sector during MIS 5e could therefore help

375   explain the differing WSI retreat in this region, with greater poleward migration of the ACC and

376   reduction in the Ross Sea gyre extent in the western Pacific sector than in the eastern Pacific sector.

377   However, unlike in the Indian sector, there is no evidence for millennial-scale migration of the ACC

378   across the Pacific sector. The stable and persistent WSIE in the Pacific sector during MIS 5e may have

379   protected ice shelves in the Ross, Amundsen and Bellingshausen seas which buttressed ice grounded

380   further upstream (Massom et al., 2018). This buttressing may have acted as a stabilising factor for the

381   West Antarctic Ice Sheet during MIS 5e, with the majority of its deep subglacial basins terminating in

382   the Ross, Amundsen and Bellingshausen Seas (Gardner et al., 2018).

383   The sensitivity of Weddell Sea WSI to warmer climates could have substantial implications for the SO

384   biosphere given the high rates of primary productivity in this region today (Vernet et al., 2019). Whilst

385   a future reduction in WSIE and increase in glacial meltwater flux would be expected to promote

386   primary productivity in the western part of the Weddell Sea (de Jong et al., 2012), the higher SSTs

387 would not favour key trophic intermediaries, e.g. Antarctic krill (*Euphausia superba*) (Atkinson et al.,

388 2017; Siegel and Watkins, 2016), and would therefore negatively affect megafauna at higher trophic

389 levels (Hill et al., 2013). Future WSI edge retreat, at equivalent levels to MIS 5e, would also negatively

390 impact upon modern sea-ice obligate species, such as Emperor and Adélie Penguins (Cimino et al.,

391 2013; Jenouvrier et al., 2005).

392 Similarly to the modern SO (Parkinson, 2019), WSIE trends during MIS 5e show both spatial and

393 temporal heterogeneity. The greater MIS 5e WSIE reduction in the Atlantic sector compared to the

394 Pacific sector is consistent with recent model simulations (Holloway et al., 2017). Most of the core

395 records in this study reach their minimum WSIE synchronously (within chronological uncertainties)

396 with the 128 ± 1.5 ka minimum in Antarctic ice core Na_{ss} flux (Wolff et al., 2006), with only cores

397 TPC290 and U1361A indicating a later WSIE minimum (Figure 3 & Supplementary Figure 1). The

398 stability of the Pacific sector WSIE is likely due to the bathymetric pinning of the ACC limiting the

399 possible poleward displacement of the ACC during MIS 5e. The apparent high sensitivity of Weddell

400 Sea WSIE, and seeming resilience of Bellingshausen Sea WSIE, to warmer than present climates is

401 unexpected from the recent observational trends (Hobbs et al., 2016; Parkinson, 2019) and highlights

402 the importance of reconstructing palaeoenvironmental conditions around Antarctica during past

403 warm periods, such as MIS 5e, for understanding how the Antarctic and SO regions respond to warmer

404 climates on longer than decadal timescales.

405 **Data availability**

406 Full diatom count data for all samples are available from the NERC EDS UK Polar Data Centre (Chadwick

407 and Allen, 2021a, b, c, d, e, f, g, h, i). Sept. SIC and SSST data for all samples, produced using the MAT

408 transfer function, are available from PANGAEA (submitted, doi pending).

409 **Author contribution**

410 **MC** – Data Curation, Investigation, Visualization, Writing – original draft preparation; **CA** –

411 Conceptualization, Project administration, Resources, Supervision, Writing – review & editing; **LS** –

412 Conceptualization, Supervision, Writing – review & editing; **XC** – Formal analysis, Methodology,

413 Resources, Writing – review & editing; **CDH** – Resources, Writing – review & editing.

414 **Competing interests**

415 The authors declare they have no conflict of interest.

416   **Acknowledgements**

417   Funding for this work was provided by The Natural Environmental Research Council [grant number

418   NE/L002531/1]. The British Ocean Sediment Core Research Facility (BOSCORF) is thanked for supplying

419   sediment samples for core TPC287. We thank the Lamont-Doherty Core Repository of Lamont-Doherty

420   Earth Observatory for providing sediment sample material for core NBP9802-04 (IGSN – DSR0003YW).

421   The International Ocean Discovery Program (IODP) is thanked for providing the sample material for

422   core U1361A. We also thank the Oregon State University Marine and Geology Repository for providing

423   sediment samples for core ELT17-9 and the Istituto de Scienze Marine for providing sediment samples

424   for core ANTA91-8.

425   **References**

426   Abernathey, R. P., Cerovecki, I., Holland, P. R., Newsom, E., Mazloff, M., and Talley, L. D.: Water-mass
427   transformation by sea ice in the upper branch of the Southern Ocean overturning, Nature
428   Geoscience, 9, 596-601, 2016.

429   Armand, L. and Leventer, A.: Palaeo sea ice distribution and reconstruction derived from the
430   geological records. In: Sea Ice, 2nd edition, Thomas, D. N. and Dieckmann, G. S. (Eds.), Wiley-
431   Blackwell, 2010.

432   Armand, L. K., Crosta, X., Romero, O., and Pichon, J.-J.: The biogeography of major diatom taxa in
433   Southern Ocean sediments: 1. Sea ice related species, Palaeogeography, Palaeoclimatology,
434   Palaeoecology, 223, 93-126, 2005.

435   Atkinson, A., Hill, S. L., Pakhomov, E. A., Siegel, V., Anadon, R., Chiba, S., Daly, K. L., Downie, R.,
436   Fielding, S., Fretwell, P., Gerrish, L., Hosie, G. W., Jessopp, M. J., Kawaguchi, S., Krafft, B. A., Loeb, V.,
437   Nishikawa, J., Peat, H. J., Reiss, C. S., Ross, R. M., Quetin, L. B., Schmidt, K., Steinberg, D. K.,
438   Subramaniam, R. C., Tarling, G. A., and Ward, P.: KRILLBASE: a circumpolar database of Antarctic krill
439   and salp numerical densities, 1926–2016, Earth System Science Data, 9, 193-210, 2017.

440   Bareille, G., Grousset, F. E., Labracherie, M., Labeyrie, L. D., and Petit, J.-R.: Origin of detrital fluxes in
441   the southeast Indian Ocean during the last climatic cycles, Paleoceanography, 9, 799-819, 1994.

442   Bazin, L., Landais, A., Lemieux-Dudon, B., Toyé Mahamadou Kele, H., Veres, D., Parrenin, F.,
443   Martinerie, P., Ritz, C., Capron, E., Lipenkov, V., Loutre, M. F., Raynaud, D., Vinther, B., Svensson, A.,
444   Rasmussen, S. O., Severi, M., Blunier, T., Leuenberger, M., Fischer, H., Masson-Delmotte, V.,
445   Chappellaz, J., and Wolff, E.: An optimized multi-proxy, multi-site Antarctic ice and gas orbital
446   chronology (AICC2012): 120-800 ka, Climate of the Past, 9, 1715-1731, 2013.

447   Benz, V., Esper, O., Gersonde, R., Lamy, F., and Tiedemann, R.: Last Glacial Maximum sea surface
448   temperature and sea-ice extent in the Pacific sector of the Southern Ocean, Quaternary Science
449   Reviews, 146, 216-237, 2016.

450   Bianchi, C. and Gersonde, R.: The Southern Ocean surface between Marine Isotope Stages 6 and 5d:
451   Shape and timing of climate changes, Palaeogeography, Palaeoclimatology, Palaeoecology, 187, 151-
452   177, 2002.

453   Bintanja, R., van Oldenborgh, G. J., Drijfhout, S. S., Wouters, B., and Katsman, C. A.: Important role
454   for ocean warming and increased ice-shelf melt in Antarctic sea-ice expansion, Nature Geoscience, 6,
455   376-379, 2013.

456   Bouttes, N., Paillard, D., and Roche, D. M.: Impact of brine-induced stratification on the glacial
457   carbon cycle, Climate of the Past, 6, 575-589, 2010.

458   Brambati, A., Melis, R., Quaia, T., and Salvi, G.: Late Quaternary climatic changes in the Ross Sea
459   area, Antarctica. In: Antarctica at the close of a Millenium, Gamble, J. A., Skinner, D. N. B., and
460   Henrys, S. (Eds.), Proceedings Volume 8th International Symposium on Antarctic Earth Sciences,
461   Royal Society of New Zealand Bulletin, 2002.

462   Burckle, L. H., Robinson, D., and Cooke, D.: Reappraisal of sea-ice distribution in Atlantic and Pacific
463   sectors of the Southern Ocean at 18,000 yr BP, Nature, 299, 435-437, 1982.

464   Capron, E., Govin, A., Feng, R., Otto-Bliesner, B. L., and Wolff, E. W.: Critical evaluation of climate
465   syntheses to benchmark CMIP6/PMIP4 127 ka Last Interglacial simulations in the high-latitude
466   regions, Quaternary Science Reviews, 168, 137-150, 2017.

467   Capron, E., Govin, A., Stone, E. J., Masson-Delmotte, V., Mulitza, S., Otto-Bliesner, B., Rasmussen, T.
468   L., Sime, L. C., Waelbroeck, C., and Wolff, E. W.: Temporal and spatial structure of multi-millennial
469   temperature changes at high latitudes during the Last Interglacial, Quaternary Science Reviews, 103,
470   116-133, 2014.

471   Ceccaroni, L., Frank, M., Frignani, M., Langone, L., Ravaioli, M., and Mangini, A.: Late Quaternary
472   fluctuations of biogenic component fluxes on the continental slope of the Ross Sea, Antarctica,
473   Journal of Marine Systems, 17, 515-525, 1998.

474   Chadwick, M.: Southern Ocean surface sediment diatom abundances. In: Mendeley Data, Mendeley
475   Data, 2020.

476   Chadwick, M. and Allen, C. S.: Marine Isotope Stage 5e diatom assemblages in marine sediment core
477   ANTA91-8 (-70.78 °N, 172.83 °E, Cruise ANTA91) - VERSION 2. NERC EDS UK Polar Data Centre,
478   2021a.

479   Chadwick, M. and Allen, C. S.: Marine Isotope Stage 5e diatom assemblages in marine sediment core
480   ELT17-9 (-63.08 °N, -135.12 °E, Cruise ELT17). UK Polar Data Centre, Natural Environment Research
481   Council, UK Research & Innovation, 2021b.

482   Chadwick, M. and Allen, C. S.: Marine Isotope Stage 5e diatom assemblages in marine sediment core
483   MD03-2603 (-64.28 °N, 139.38 °E, Cruise MD130) UK Polar Data Centre, Natural Environment
484   Research Council, UK Research & Innovation, 2021c.

485   Chadwick, M. and Allen, C. S.: Marine Isotope Stage 5e diatom assemblages in marine sediment core
486   NBP9802-04 (-64.20 °N, -170.08 °E, Cruise PA9802) UK Polar Data Centre, Natural Environment
487   Research Council, UK Research & Innovation, 2021d.

488   Chadwick, M. and Allen, C. S.: Marine Isotope Stage 5e diatom assemblages in marine sediment core
489   PC509 (-68.31 °N, -86.03 °E, Cruise JR179). UK Polar Data Centre, Natural Environment Research
490   Council, UK Research & Innovation, 2021e.

491   Chadwick, M. and Allen, C. S.: Marine Isotope Stage 5e diatom assemblages in marine sediment core
492   TPC287 (-60.31 °N, -36.65 °E, Cruise JR48) UK Polar Data Centre, Natural Environment Research
493   Council, UK Research & Innovation, 2021f.

494   Chadwick, M. and Allen, C. S.: Marine Isotope Stage 5e diatom assemblages in marine sediment core
495   TPC288 (-59.14 °N, -37.96 °E, Cruise JR48) UK Polar Data Centre, Natural Environment Research
496   Council, UK Research & Innovation, 2021g.

497   Chadwick, M. and Allen, C. S.: Marine Isotope Stage 5e diatom assemblages in marine sediment core
498   TPC290 (-55.55 °N, -45.02 °E, Cruise JR48). UK Polar Data Centre, Natural Environment Research
499   Council, UK Research & Innovation, 2021h.

500   Chadwick, M. and Allen, C. S.: Marine Isotope Stage 5e diatom assemblages in marine sediment core
501   U1361A (-64.41 °N, 143.89 °E, IODP Exp. 318) UK Polar Data Centre, Natural Environment Research
502   Council, UK Research & Innovation, 2021i.

503   Chadwick, M., Allen, C. S., Sime, L. C., and Crosta, X.: How does the Southern Ocean
504   palaeoenvironment during MIS 5e compare to the modern?, Marine Micropaleontology, *in review*. *in*
505   *review*.

506   Chadwick, M., Allen, C. S., Sime, L. C., and Hillenbrand, C. D.: Analysing the timing of peak warming
507   and minimum winter sea-ice extent in the Southern Ocean during MIS 5e, Quaternary Science
508   Reviews, 229, 106134, 2020.

509   Chase, Z., Anderson, R. F., Fleisher, M. Q., and Kubik, P. W.: Accumulation of biogenic and lithogenic
510   material in the Pacific sector of the Southern Ocean during the past 40,000 years, Deep Sea Research
511   Part II: Topical Studies in Oceanography, 50, 799-832, 2003.

512   Cimino, M. A., Fraser, W. R., Irwin, A. J., and Oliver, M. J.: Satellite data identify decadal trends in the
513   quality of Pygoscelis penguin chick-rearing habitat, Glob Chang Biol, 19, 136-148, 2013.

514   Cremer, H., Roberts, D., McMinn, A., Gore, D., and Melles, M.: The Holocene Diatom Flora of Marine
515   Bays in the Windmill Islands, East Antarctica, Botanica Marina, 46, 82-106, 2003.

516   Crosta, X., Pichon, J.-J., and Labracherie, M.: Distribution of *Chaetoceros* resting spores in modern
517   peri-Antarctic sediments, Marine Micropaleontology, 29, 283-299, 1997.

518   Crosta, X., Romero, O., Armand, L. K., and Pichon, J.-J.: The biogeography of major diatom taxa in
519   Southern Ocean sediments: 2. Open ocean related species, Palaeogeography, Palaeoclimatology,
520   Palaeoecology, 223, 66-92, 2005.

521   Crosta, X., Shukla, S. K., Ther, O., Ikehara, M., Yamane, M., and Yokoyama, Y.: Last Abundant
522   Appearance Datum of Hemidiscus karstenii driven by climate change, Marine Micropaleontology,
523   157, 101861, 2020.

524   CSIRO: State of the Climate, Bureau of Meteorology, Australia, 1-24 pp., 2018.

525   de Jong, J., Schoemann, V., Lannuzel, D., Croot, P., de Baar, H., and Tison, J.-L.: Natural iron
526   fertilization of the Atlantic sector of the Southern Ocean by continental shelf sources of the Antarctic
527   Peninsula, Journal of Geophysical Research: Biogeosciences, 117, 2012.

528   Dotto, T. S., Naveira Garabato, A., Bacon, S., Tsamados, M., Holland, P. R., Hooley, J., Frajka-Williams,
529   E., Ridout, A., and Meredith, M. P.: Variability of the Ross Gyre, Southern Ocean: Drivers and
530   Responses Revealed by Satellite Altimetry, Geophysical Research Letters, 45, 6195-6204, 2018.

531   Esper, O., Gersonde, R., and Kadagies, N.: Diatom distribution in southeastern Pacific surface
532   sediments and their relationship to modern environmental variables, Palaeogeography,
533   Palaeoclimatology, Palaeoecology, 287, 1-27, 2010.

534   Ferreira, D., Marshall, J., Bitz, C. M., Solomon, S., and Plumb, A.: Antarctic Ocean and Sea Ice
535   Response to Ozone Depletion: A Two-Time-Scale Problem, Journal of Climate, 28, 1206-1226, 2015.

536   Fetterer, F., Knowles, K., Meier, W. N., Savoie, M., and Windnagel, A. K.: Sea Ice Index, Version 3.
537   NSIDC: National Snow and Ice Data Center, Boulder, Colorado USA, 2017.

538   Fischer, H., Meissner, K. J., Mix, A. C., Abram, N. J., Austermann, J., Brovkin, V., Capron, E.,
539   Colombaroli, D., Daniau, A.-L., Dyez, K. A., Felis, T., Finkelstein, S. A., Jaccard, S. L., McClymont, E. L.,
540   Rovere, A., Sutter, J., Wolff, E. W., Affolter, S., Bakker, P., Ballesteros-Cánovas, J. A., Barbante, C.,
541   Caley, T., Carlson, A. E., Churakova, O., Cortese, G., Cumming, B. F., Davis, B. A. S., de Vernal, A.,
542   Emile-Geay, J., Fritz, S. C., Gierz, P., Gottschalk, J., Holloway, M. D., Joos, F., Kucera, M., Loutre, M.-F.,
543   Lunt, D. J., Marcisz, K., Marlon, J. R., Martinez, P., Masson-Delmotte, V., Nehrbass-Ahles, C., Otto-
544   Bliesner, B. L., Raible, C. C., Risebrobakken, B., Sánchez Goñi, M. F., Arrigo, J. S., Sarnthein, M., Sjolte,
545   J., Stocker, T. F., Velasquez Alvárez, P. A., Tinner, W., Valdes, P. J., Vogel, H., Wanner, H., Yan, Q., Yu,
546   Z., Ziegler, M., and Zhou, L.: Palaeoclimate constraints on the impact of 2 °C anthropogenic warming
547   and beyond, Nature Geoscience, 11, 474-485, 2018.

548   Fogwill, C. J., Turney, C. S. M., Meissner, K. J., Golledge, N. R., Spence, P., Roberts, J. L., England, M.
549   H., Jones, R. T., and Carter, L.: Testing the sensitivity of the East Antarctic Ice Sheet to Southern
550   Ocean dynamics: past changes and future implications, Journal of Quaternary Science, 29, 91-98,
551   2014.

552   Gardner, A. S., Moholdt, G., Scambos, T., Fahnstock, M., Ligtenberg, S., van den Broeke, M., and
553   Nilsson, J.: Increased West Antarctic and unchanged East Antarctic ice discharge over the last 7
554   years, The Cryosphere, 12, 521-547, 2018.

555   Gersonde, R., Crosta, X., Abelmann, A., and Armand, L.: Sea-surface temperature and sea ice
556   distribution of the Southern Ocean at the EPILOG Last Glacial Maximum—a circum-Antarctic view
557   based on siliceous microfossil records, Quaternary Science Reviews, 24, 869-896, 2005.

558   Gersonde, R. and Zielinski, U.: The reconstruction of late Quaternary Antarctic sea-ice distribution—
559   the use of diatoms as a proxy for sea-ice, Palaeogeography, Palaeoclimatology, Palaeoecology, 162,
560   263-286, 2000.

561   Goosse, H. and Zunz, V.: Decadal trends in the Antarctic sea ice extent ultimately controlled by ice–
562   ocean feedback, The Cryosphere, 8, 453-470, 2014.

563   Govin, A., Braconnot, P., Capron, E., Cortijo, E., Duplessy, J. C., Jansen, E., Labeyrie, L., Landais, A.,
564   Marti, O., Michel, E., Mosquet, E., Risebrobakken, B., Swingedouw, D., and Waelbroeck, C.:
565   Persistent influence of ice sheet melting on high northern latitude climate during the early Last
566   Interglacial, Climate of the Past, 8, 483-507, 2012.

567   Govin, A., Capron, E., Tzedakis, P. C., Verheyden, S., Ghaleb, B., Hillaire-Marcel, C., St-Onge, G.,
568   Stoner, J. S., Bassinot, F., Bazin, L., Blunier, T., Combourieu-Nebout, N., El Ouahabi, A., Genty, D.,
569   Gersonde, R., Jimenez-Amat, P., Landais, A., Martrat, B., Masson-Delmotte, V., Parrenin, F.,

570 Seidenkrantz, M. S., Veres, D., Waelbroeck, C., and Zahn, R.: Sequence of events from the onset to
571 the demise of the Last Interglacial: Evaluating strengths and limitations of chronologies used in
572 climatic archives, Quaternary Science Reviews, 129, 1-36, 2015.

573 Govin, A., Michel, E., Labeyrie, L., Waelbroeck, C., Dewilde, F., and Jansen, E.: Evidence for
574 northward expansion of Antarctic Bottom Water mass in the Southern Ocean during the last glacial
575 inception, Paleoceanography, 24, PA1202, 2009.

576 Guiot, J. and de Vernal, A.: Is spatial autocorrelation introducing biases in the apparent accuracy of
577 paleoclimatic reconstructions?, Quaternary Science Reviews, 30, 1965-1972, 2011.

578 Hall, A.: The Role of Surface Albedo Feedback in Climate, Journal of Climate, 17, 1550-1568, 2004.

579 Hellmer, H. H., Kauker, F., Timmermann, R., Determann, J., and Rae, J.: Twenty-first-century warming
580 of a large Antarctic ice-shelf cavity by a redirected coastal current, Nature, 485, 225-228, 2012.

581 Hersbach, H., Bell, B., Berrisford, P., Biavati, G., Horanyi, A., Munoz Sabater, J., Nicolas, J., Peubey, C.,
582 Radu, R., Rozum, I., Schepers, D., Simmons, A., Soci, C., Dee, D., and Thepaut, J.-N.: ERA5 monthly
583 averaged data on single levels from 1980 to 2019., Copernicus Climate Change Service (C3S) Climate
584 Data Store (CDS), 2019.

585 Hill, S. L., Phillips, T., and Atkinson, A.: Potential Climate Change Effects on the Habitat of Antarctic
586 Krill in the Weddell Quadrant of the Southern Ocean, PLoS One, 8, e72246, 2013.

587 Hobbs, W. R., Massom, R., Stammerjohn, S., Reid, P., Williams, G., and Meier, W.: A review of recent
588 changes in Southern Ocean sea ice, their drivers and forcings, Global and Planetary Change, 143,
589 228-250, 2016.

590 Holloway, M. D., Sime, L. C., Allen, C. S., Hillenbrand, C.-D., Bunch, P., Wolff, E., and Valdes, P. J.: The
591 spatial structure of the 128 ka Antarctic sea ice minimum, Geophysical Research Letters, 44, 11129-
592 11139, 2017.

593 Holloway, M. D., Sime, L. C., Singarayer, J. S., Tindall, J. C., and Valdes, P. J.: Simulating the 128-ka
594 Antarctic Climate Response to Northern Hemisphere Ice Sheet Melting Using the Isotope-Enabled
595 HadCM3, Geophysical Research Letters, 45, 11,921-911,929, 2018.

596 IPCC: Summary for Policymakers. In: IPCC Special Report on the Ocean and Cryosphere in a Changing
597 Climate, Portner, H. O., Roberts, D. C., Masson-Delmotte, V., Zhai, P., Tignor, M., Poloczanska, E.,
598 Mintenbeck, K., Alegria, A., Nicolai, M., Okem, A., Petzold, J., Rama, B., and Weyers, N. M. (Eds.),
599 2019.

600 Jenouvrier, S., Barbraud, C., and Weimerskirch, H.: Long-term contrasted responses to climate of two
601 Antarctic seabird species, Ecology, 86, 2889-2903, 2005.

602 Kim, S., Lee, J. I., McKay, R. M., Yoo, K.-C., Bak, Y.-S., Lee, M. K., Roh, Y. H., Yoon, H. I., Moon, H. S.,
603 and Hyun, C.-U.: Late pleistocene paleoceanographic changes in the Ross Sea – Glacial-interglacial
604 variations in paleoproductivity, nutrient utilization, and deep-water formation, Quaternary Science
605 Reviews, 239, 106356, 2020.

606 King, J.: A resolution of the Antarctic paradox, Nature, 505, 491-492, 2014.

607 Kopp, R. E., Simons, F. J., Mitrovica, J. X., Maloof, A. C., and Oppenheimer, M.: Probabilistic
608 assessment of sea level during the last interglacial stage, Nature, 462, 863-867, 2009.

609   Kopp, R. E., Simons, F. J., Mitrovica, J. X., Maloof, A. C., and Oppenheimer, M.: A probabilistic
610   assessment of sea level variations within the last interglacial stage, Geophysical Journal
611   International, 193, 711-716, 2013.

612   Lisiecki, L. E. and Raymo, M. E.: A Pliocene-Pleistocene stack of 57 globally distributed benthic δ18O
613   records, Paleoceanography, 20, PA1003, 2005.

614   Liu, J. and Curry, J. A.: Accelerated warming of the Southern Ocean and its impacts on the
615   hydrological cycle and sea ice, Proc Natl Acad Sci U S A, 107, 14987-14992, 2010.

616   Locarnini, R. A., Mishonov, A. V., Antonov, J. I., Boyer, T. P., Garcia, H. E., Baranova, O. K., Zweng, M.
617   M., Paver, C. R., Reagan, J. R., Johnson, D. R., Hamilton, M., and Seidov, D.: World Ocean atlas 2013,
618   volume 1: Temperature, 2013.

619   Maksym, T.: Arctic and Antarctic Sea Ice Change: Contrasts, Commonalities, and Causes, Ann Rev
620   Mar Sci, 11, 187-213, 2019.

621   Marzocchi, A. and Jansen, M. F.: Global cooling linked to increased glacial carbon storage via changes
622   in Antarctic sea ice, Nature Geoscience, 12, 1001-1005, 2019.

623   Massom, R. A., Scambos, T. A., Bennetts, L. G., Reid, P., Squire, V. A., and Stammerjohn, S. E.:
624   Antarctic ice shelf disintegration triggered by sea ice loss and ocean swell, Nature, 558, 383-389,
625   2018.

626   Meredith, M., Sommerkorn, M., Cassotta, S., Derksen, C., Ekaykin, A., Hollowed, A., Kofinas, G.,
627   Mackintosh, A., Melbourne-Thomas, J., Muelbert, M. M. C., Ottersen, G., Pritchard, H., and Schuur,
628   E. A. G.: Polar Regions. In: IPCC Special Report on the Ocean and Cryosphere in a Changing Climate,
629   Portner, H. O., Roberts, D. C., Masson-Delmotte, V., Zhai, P., Tignor, M., Poloczanska, E., Mintenbeck,
630   K., Alegria, A., Nicolai, M., Okem, A., Petzold, J., Rama, B., and Weyers, N. M. (Eds.), 2019.

631   Merino, N., Jourdain, N. C., Le Sommer, J., Goosse, H., Mathiot, P., and Durand, G.: Impact of
632   increasing antarctic glacial freshwater release on regional sea-ice cover in the Southern Ocean,
633   Ocean Modelling, 121, 76-89, 2018.

634   Merino, N., Le Sommer, J., Durand, G., Jourdain, N. C., Madec, G., Mathiot, P., and Tournadre, J.:
635   Antarctic icebergs melt over the Southern Ocean: Climatology and impact on sea ice, Ocean
636   Modelling, 104, 99-110, 2016.

637   Nghiem, S. V., Rigor, I. G., Clemente-Colón, P., Neumann, G., and Li, P. P.: Geophysical constraints on
638   the Antarctic sea ice cover, Remote Sensing of Environment, 181, 281-292, 2016.

639   Paillard, D., Labeyrie, L., and Yiou, P.: Macintosh program performs time-series analysis, Eos, 77, 379,
640   1996.

641   Parkinson, C. L.: A 40-y record reveals gradual Antarctic sea ice increases followed by decreases at
642   rates far exceeding the rates seen in the Arctic, Proc Natl Acad Sci USA, 116, 14414-14423, 2019.

643   Parrenin, F., Masson-Delmotte, V., Kohler, P., Raynaud, D., Paillard, D., Schwander, J., Barbante, C.,
644   Landais, A., Wegner, A., and Jouzel, J.: Synchronisation of the LR04 stack with EDC isotopic variations
645   on the EDC3 age scale. In: PANGAEA, 2013.

646 Presti, M., Barbara, L., Denis, D., Schmidt, S., De Santis, L., and Crosta, X.: Sediment delivery and
647 depositional patterns off Adélie Land (East Antarctica) in relation to late Quaternary climatic cycles,
648 Marine Geology, 284, 96-113, 2011.

649 Pugh, R. S., McCave, I. N., Hillenbrand, C. D., and Kuhn, G.: Circum-Antarctic age modelling of
650 Quaternary marine cores under the Antarctic Circumpolar Current: Ice-core dust–magnetic
651 correlation, Earth and Planetary Science Letters, 284, 113-123, 2009.

652 Purich, A., England, M. H., Cai, W., Chikamoto, Y., Timmermann, A., Fyfe, J. C., Frankcombe, L.,
653 Meehl, G. A., and Arblaster, J. M.: Tropical Pacific SST Drivers of Recent Antarctic Sea Ice Trends,
654 Journal of Climate, 29, 8931-8948, 2016.

655 Rignot, E., Mouginot, J., Scheuchl, B., van den Broeke, M., van Wessem, M. J., and Morlighem, M.:
656 Four decades of Antarctic Ice Sheet mass balance from 1979-2017, Proc Natl Acad Sci U S A, 116,
657 1095-1103, 2019.

658 Rintoul, S. R.: The global influence of localized dynamics in the Southern Ocean, Nature, 558, 209-
659 218, 2018.

660 Romero, O. E., Armand, L. K., Crosta, X., and Pichon, J. J.: The biogeography of major diatom taxa in
661 Southern Ocean surface sediments: 3. Tropical/Subtropical species, Palaeogeography,
662 Palaeoclimatology, Palaeoecology, 223, 49-65, 2005.

663 Rosenblum, E. and Eisenman, I.: Sea Ice Trends in Climate Models Only Accurate in Runs with Biased
664 Global Warming, Journal of Climate, 30, 6265-6278, 2017.

665 Rysgaard, S., Bendtsen, J., Delille, B., Dieckmann, G. S., Glud, R. N., Kennedy, H., Mortensen, J.,
666 Papadimitriou, S., Thomas, D. N., and Tison, J.-L.: Sea ice contribution to the air–sea CO_2 exchange in
667 the Arctic and Southern Oceans, Tellus B: Chemical and Physical Meteorology, 63, 823-830, 2011.

668 Saunders, K. M., Kamenik, C., Hodgson, D. A., Hunziker, S., Siffert, L., Fischer, D., Fujak, M., Gibson, J.
669 A. E., and Grosjean, M.: Late Holocene changes in precipitation in northwest Tasmania and their
670 potential links to shifts in the Southern Hemisphere westerly winds, Global and Planetary Change,
671 92-93, 82-91, 2012.

672 Scherer, R. P.: A new method for the determination of absolute abundance of diatoms and other silt-
673 sized sedimentary particles, Journal of Paleolimnology, 12, 171-179, 1994.

674 Schweitzer, P. N.: Monthly average polar sea-ice concentration 1978 through 1991. In: U.S.
675 Geological Survey Digital Data Series DDS-27, U.S. Geological Survey, Reston, Virginia, 1995.

676 Shukla, S. K., Crosta, X., and Ikehara, M.: Sea Surface Temperatures in the Indian Sub-Antarctic
677 Southern Ocean for the Last Four Interglacial Periods, Geophysical Research Letters, 48, 2021.

678 Siegel, V. and Watkins, J. L.: Distribution, Biomass and Demography of Antarctic Krill, *Euphausia*
679 *superba*. In: Biology and Ecology of Antarctic krill, Siegel, V. (Ed.), Advances in Polar Ecology, 2016.

680 Sime, L. C., Carlson, A. E., and Holloway, M. D.: On recovering Last Interglacial changes in the
681 Antarctic ice sheet, Past Global Changes Magazine, 27, 14-15, 2019.

682 Simpson, G.: Analogue Methods in Palaeoecology: Using the analogue Package, Journal of Statistical
683 Software, 22, i02, 2007.

684 Stammerjohn, S. E., Martinson, D. G., Smith, R. C., Yuan, X., and Rind, D.: Trends in Antarctic annual
685 sea ice retreat and advance and their relation to El Niño–Southern Oscillation and Southern Annular
686 Mode variability, Journal of Geophysical Research, 113, C03S90, 2008.

687 Stone, E. J., Capron, E., Lunt, D. J., Payne, A. J., Singarayer, J. S., Valdes, P. J., and Wolff, E. W.: Impact
688 of meltwater on high-latitude early Last Interglacial climate, Climate of the Past, 12, 1919-1932,
689 2016.

690 Tamsitt, V., Drake, H. F., Morrison, A. K., Talley, L. D., Dufour, C. O., Gray, A. R., Griffies, S. M.,
691 Mazloff, M. R., Sarmiento, J. L., Wang, J., and Weijer, W.: Spiraling pathways of global deep waters to
692 the surface of the Southern Ocean, Nat Commun, 8, 172, 2017.

693 Thomas, E. R., Allen, C. S., Etourneau, J., King, A. C. F., Severi, M., Winton, V. H. L., Mueller, J., Crosta,
694 X., and Peck, V. L.: Antarctic Sea Ice Proxies from Marine and Ice Core Archives Suitable for
695 Reconstructing Sea Ice over the Past 2000 Years, Geosciences, 9, 506, 2019.

696 Trathan, P. N., Brandon, M. A., Murphy, E. J., and Thorpe, S. E.: Transport and structure within the
697 Antarctic Circumpolar Current to the north of south Georgia, Geophysical Research Letters, 27,
698 1727-1730, 2000.

699 Turney, C. S. M., Fogwill, C. J., Golledge, N. R., McKay, N. P., van Sebille, E., Jones, R. T., Etheridge, D.,
700 Rubino, M., Thornton, D. P., Davies, S. M., Ramsey, C. B., Thomas, Z. A., Bird, M. I., Munksgaard, N.
701 C., Kohno, M., Woodward, J., Winter, K., Weyrich, L. S., Rootes, C. M., Millman, H., Albert, P. G.,
702 Rivera, A., van Ommen, T., Curran, M., Moy, A., Rahmstorf, S., Kawamura, K., Hillenbrand, C. D.,
703 Weber, M. E., Manning, C. J., Young, J., and Cooper, A.: Early Last Interglacial ocean warming drove
704 substantial ice mass loss from Antarctica, Proc Natl Acad Sci U S A, 117, 3996-4006, 2020.

705 Veres, D., Bazin, L., Landais, A., Toyé Mahamadou Kele, H., Lemieux-Dudon, B., Parrenin, F.,
706 Martinerie, P., Blayo, E., Blunier, T., Capron, E., Chappellaz, J., Rasmussen, S. O., Severi, M.,
707 Svensson, A., Vinther, B., and Wolff, E. W.: The Antarctic ice core chronology (AICC2012): an
708 optimized multi-parameter and multi-site dating approach for the last 120 thousand years, Climate
709 of the Past, 9, 1733-1748, 2013.

710 Vernet, M., Geibert, W., Hoppema, M., Brown, P. J., Haas, C., Hellmer, H. H., Jokat, W., Jullion, L.,
711 Mazloff, M., Bakker, D. C. E., Brearley, J. A., Croot, P., Hattermann, T., Hauck, J., Hillenbrand, C. D.,
712 Hoppe, C. J. M., Huhn, O., Koch, B. P., Lechtenfeld, O. J., Meredith, M. P., Naveira Garabato, A. C.,
713 Nöthig, E. M., Peeken, I., Rutgers van der Loeff, M. M., Schmidtko, S., Schröder, M., Strass, V. H.,
714 Torres-Valdés, S., and Verdy, A.: The Weddell Gyre, Southern Ocean: Present Knowledge and Future
715 Challenges, Reviews of Geophysics, 57, 623-708, 2019.

716 von Quillfeldt, C.: The diatom *Fragilariopsis cylindrus* and its potential as an indicator species for cold
717 water rather than for sea ice, Vie et Milieu / Life & Environment, 54, 137-143, 2004.

718 Wahlin, A. K., Graham, A. G. C., Hogan, K. A., Queste, B. Y., Boehme, L., Larter, R. D., Pettit, E. C.,
719 Wellner, J., and Heywood, K. J.: Pathways and modification of warm water flowing beneath Thwaites
720 Ice Shelf, West Antarctica, Science Advances, 7, eabd7254, 2021.

721 Walter, H. J., Hegner, E., Diekmann, B., Kuhn, G., and Rutgers van der Loeff, M. M.: Provenance and
722 transport of terrigenous sediment in the South Atlantic Ocean and their relations to glacial and
723 interglacial cycles: Nd and Sr isotopic evidence, Geochimica et Cosmochimica Acta, 64, 3813-3827,
724 2000.

725 Williams, T.: Investigating the circulation of Southern Ocean deep water masses over the last 1.5
726 million years by geochemical fingerprinting of marine sediments, PhD, Department of Earth Sciences,
727 University of Cambridge, UK, 210 pp., 2017.

728 Wilson, D. J., Bertram, R. A., Needham, E. F., van de Flierdt, T., Welsh, K. J., McKay, R. M., Mazumder,
729 A., Riesselman, C. R., Jimenez-Espejo, F. J., and Escutia, C.: Ice loss from the East Antarctic Ice Sheet
730 during late Pleistocene interglacials, Nature, 561, 383-386, 2018.

731 Wolff, E. W., Fischer, H., Fundel, F., Ruth, U., Twarloh, B., Littot, G. C., Mulvaney, R., Rothlisberger,
732 R., de Angelis, M., Boutron, C. F., Hansson, M., Jonsell, U., Hutterli, M. A., Lambert, F., Kaufmann, P.,
733 Stauffer, B., Stocker, T. F., Steffensen, J. P., Bigler, M., Siggaard-Andersen, M. L., Udisti, R., Becagli, S.,
734 Castellano, E., Severi, M., Wagenbach, D., Barbante, C., Gabrielli, P., and Gaspari, V.: Southern Ocean
735 sea-ice extent, productivity and iron flux over the past eight glacial cycles, Nature, 440, 491-496,
736 2006.

737 Zielinski, U., Bianchi, C., Gersonde, R., and Kunz-Pirrung, M.: Last occurrence datums of the diatoms
738 *Rouxia leventerae* and *Rouxia constricta*: indicators for marine isotope stages 6 and 8 in Southern
739 Ocean sediments, Marine Micropaleontology, 46, 127-137, 2002.

740 Zielinski, U. and Gersonde, R.: Diatom distribution in Southern Ocean surface sediments (Atlantic
741 sector): Implications for paleoenvironmental reconstructions, Palaeogeography, Palaeoclimatology,
742 Palaeoecology, 129, 213-250, 1997.

743 Zwally, H. J., Comiso, J. C., Parkinson, C. L., Cavalieri, D. J., and Gloersen, P.: Variability of Antarctic
744 sea ice 1979–1998, Journal of Geophysical Research, 107, 2002.

745